








Effect of iterative reconstruction techniques on image quality in low radiation dose chest CT: a phantom study

Yan Xu 
Ting-ting Zhang 
Zhi-hai Hu 
Juan Li 
Hong-jun Hou 
Zu-shan Xu 
Wen He 

PURPOSE

We aimed to evaluate the quality of chest computed tomography (CT) images obtained with low-dose CT using three iterative reconstruction (IR) algorithms.

METHODS

Two 64-detector spiral CT scanners (HDCT and iCT) were used to scan a chest phantom containing 6 ground-glass nodules (GGNs) at 11 radiation dose levels. CT images were reconstructed by filtered back projection or three IR algorithms. Reconstructed images were analyzed for CT values, average noise, contrast-to-noise ratio (CNR) values, subjective image noise, and diagnostic acceptability of the GGNs. Repeated-measures analysis of variance was used for statistical analyses.


RESULTS

Average noise decreased and CNR increased with increasing radiation dose when the same reconstruction algorithm was applied. Average image noise was significantly lower when reconstructed with MBIR than with iDOSE⁴ at the same low radiation doses. The two radiologists showed good interobserver consistency in image quality with kappa 0.83. A significant relationship was found between image noise and diagnostic acceptability of the GGNs.

CONCLUSION

Three IR algorithms are able to reduce the image noise and improve the image quality of low-dose CT. In the same radiation dose, the low-dose CT image quality reconstructed with MBIR algorithms is better than that of other IR algorithms.

The number of computed tomography (CT) examinations performed has increased dramatically over the past decade. Radiation exposure during CT examinations has caused widespread concern by government authorities and the public (1). The latest estimation of Global Burden of Cancer 2018 published that tracheal, bronchus, and lung cancer was the leading cause of cancer death for both males and females, with 1.6 million deaths (age-standardized death rates, 27.0 per 100,000) (2, 3). To improve diagnostic sensitivity, high radiation doses may be used, resulting in an elevated risk of cancer induced by radiation (4, 5). Recently, the National Lung Screening Trial demonstrated that three annual low-dose CT screenings (cumulative average effective dose, 4.5 mSv) resulted in a 20% relative mortality reduction of lung cancer for individuals at high risk of lung cancer (6). Several technological developments have been made to reduce radiation dose, including CT equipment enabling automatic modulation of the tube current (7, 8) and dynamic adjustment of the z-axis direction of the x-ray beam collimator (9, 10). CT images are traditionally reconstructed with filtered back projection (FBP) algorithms, which typically produce increased image noise at reduced radiation dose (11). On the contrary, the recently introduced iterative reconstruction (IR) algorithms provide much better noise performance at low radiation levels. Although CT screening to follow up benign lesions can accommodate some noise to reduce the radiation dose (12, 13), no clinical consensus exists regarding the limit of an “acceptable” amount of noise. An ideal approach would be to use low-dose parameters and IR algorithms to generate images with an acceptable noise level (13, 14). IR techniques

From the Department of Radiology (Y.X.  doctorxy08@126.com, T.Z., Z.H., J.L., W.H.), Beijing Friendship Hospital, Capital Medical University, Beijing, China; Department of Radiology (H.H., Z.X.), Weihai Wendeng Central Hospital, Weihai, Shandong, China.

Received 18 December 2018; revision requested 15 January 2019; last revision received 11 April 2019; accepted 22 April 2019.

Published online 27 September 2019.

DOI 10.5152/dir.2019.18539

You may cite this article as: Xu Y, Zhang T, Hu Z, et al. Effect of iterative reconstruction techniques on image quality in low radiation dose chest CT: a phantom study. *Diagn Interv Radiol* 2019; 25:442–450.

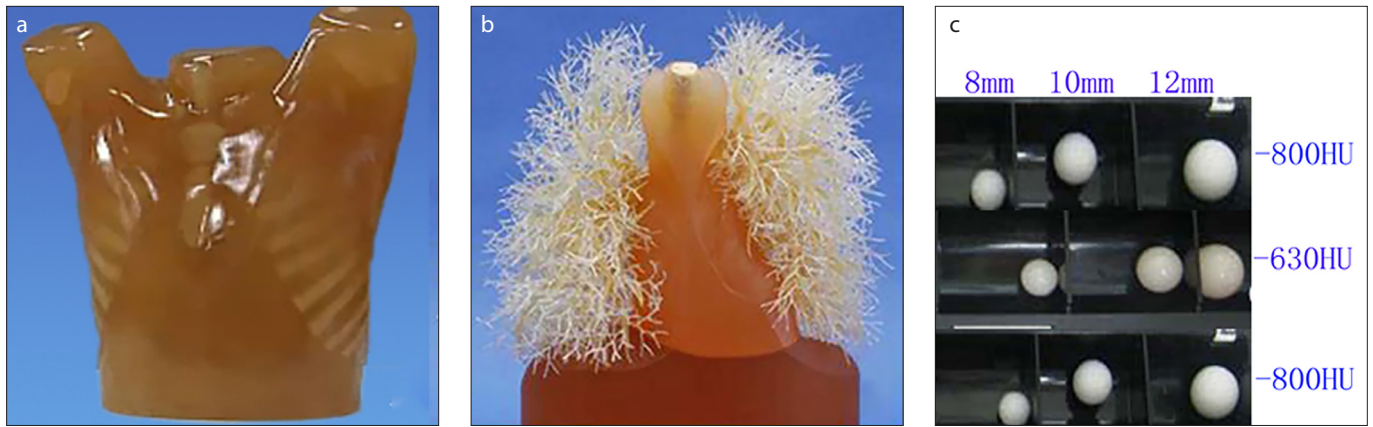


Figure 1. a–c. Panel (a) shows the external view of the chest phantom; panel (b) shows internal structure of the phantom; panel (c) shows the ground-glass nodules.

have recently been explored to improve CT image quality at low radiation doses and have good diagnostic capabilities (15–20). However, although ground-glass nodules (GGNs) are usually followed up with low-dose CT, the effect of IR algorithms in detecting GGNs has not been highlighted.

This study used an adaptive statistical IR (ASIR) algorithm, the model-based IR algorithm (MBIR, trade-name “VEO”, General Electric Company), and iDOSE⁴ (Philips Medical Company) to reconstruct the chest low-dose CT images. We aimed to evaluate the quality of chest CT images obtained with low-dose CT using three IR algorithms.

Methods

This study was exempt from institutional review board approval because no animal or human data were acquired or used.

CT scanners

A Discovery CT 750 HD (HDCT, GE Medical) and a Brilliance CT (iCT, Philips Healthcare) were used for scanning. Both CT systems were equipped with 64-row detectors and provided a collimation width of 40 mm.

Main points

- Different radiation doses reconstructed with three IR algorithms do not affect the accuracy of CT value.
- ASIR, MBIR and iDOSE⁴ algorithms are able to reduce the image noise and improve the image quality in low-dose CT.
- In the same radiation dose, the low-dose CT image quality reconstructed with MBIR algorithm is better than that of other IR algorithms.

Data were not compared between scanners, as the scanning parameters were slightly different and specific to each machine.

Chest model

The chest phantom (PH-1, Kyoto-Kagaku) was composed of polyurethane resin (SZ-50) and artificial bone. The phantom dimensions were 43×48 cm², with a bust of 94 cm. The phantom included a vertical diaphragm (representing the upper trachea), pulmonary vasculature, abdominal diaphragm, and bone (Fig. 1a, 1b). Embedded in the phantom were six GGNs, with diameters of 8, 10, and 12 mm and CT values of -800 and -600 HU (Fig. 1c). GGNs were randomly attached to the lung texture of the three lung zones of chest model (upper, above the carina; middle, between the carina and inferior pulmonary vein; lower, below the inferior pulmonary vein), but care was taken to prevent adherence to the pleura, under the pleura, or overlap with the ribs as much as possible.

CT data acquisition

The HDCT and iCT devices were used to scan the chest phantom in a fixed scan range (apex to diaphragm). Each machine acquired images at three tube currents. The HDCT scanner used automatic settings for the tube current, with noise index (NI) values of 25 for group A, 30 for group B, and 35 for group C. The iCT scanner used tube current values of 30 mAs for group D, 50 mAs for group E, and 70 mAs for group F. Two peak voltages (80 and 100 kV) were tested for each group. The scan speed was 0.5 s/circle, dynamic field of view was 36.0 cm, slice thickness was 5 mm with an interval of 5 mm, collimation width was 0.625×64 mm, and pitch was 0.984:1. The lung kernel used

for FBP of the HDCT and iCT scanners was STANDARD and B, respectively.

Images were reconstructed at 512×512 pixels. Original images were reconstructed with a section width of 0.625 mm at an interval of 0.625 mm by the 30% ASIR (commercial algorithms), MBIR (in-house algorithms), and iDOSE⁴ L3 and L6 (commercial algorithms) IR algorithms. Reconstructed images were transferred to an Extended Brilliance Workspace for analysis.

Radiation dose calculation

Recordings from both CT scanners were used to measure the dose length product (DLP, in mGy·cm) and the effective dose (ED, in mSv) with the equation $ED = DLP \times k$, where k is a weighting factor for different body regions. A k value of 0.014 mSv/mGy·cm was used for this study according to the European Quality Standards for CT Guidance for the chest (21).

Measurement of physical indicators of the image and objective evaluation of image quality

Measurements of physical indicators of the image and objective evaluations of image quality were made independently by two radiologists, each with more than 10 years of experience in chest imaging diagnosis. Each physical indicator was measured on the unenhanced CT image with lung (width, 1500 Hounsfield units (HU); level, -500 HU) and mediastinal (width, 400 HU; level, 80 HU) window settings. CT values (in HU) of the lung air and the homogeneous regions of thorax below the aortic arch at 10 consecutive levels were measured by a 100 mm² region of interest (ROI), which was placed at the center

of the measured feature in each scan, and recorded as the mean±standard deviation (SD) (18). For the objective evaluation of image quality, 15 mm² ROIs were placed on and around 6 GGNs. The mean±SD CT values

for the GGNs and background were recorded as HU_{nodule}, HU_{bkgd}, SD_{nodule}, and SD_{bkgd}, respectively. The average measurement from both radiologists was used to calculate the contrast (C) = |HU_{nodule} - HU_{bkgd}|,

the average noise (SD_{nodule/bkgd}) = (SD_{nodule} + SD_{bkgd})/2, and the contrast-to-noise ratio (CNR) = C/SD_{nodule/bkgd} (18).

Subjective evaluation of image quality

We chose eight CT images with GGN in different parts of the chest phantom with different radiation doses and reconstructed with each algorithm. Two radiologists evaluated the image quality in a blinded and random manner on a 5-megapixel 21-inch monochrome liquid-crystal display monitor. All images were displayed at a window level of 500 HU and a window width of -1500 HU. Image quality was evaluated for subjective image noise and diagnostic acceptability of the GGNs.

Subjective image noise was assessed in the lung window on a five-point scale (22, 23) as follows: 1, no or only minimal image noise; 2, below-average image noise; 3, average image noise; 4,

Group	80 kV			100 kV		
	CTDI (mGy)	DLP (mGy-cm)	ED (mSv)	CTDI (mGy)	DLP (mGy-cm)	ED (mSv)
A	1.64	55.90	0.78	1.49	50.87	0.71
B	1.13	38.65	0.54	1.03	35.17	0.49
C	0.83	28.21	0.39	0.75	25.70	0.36
D	1.59	55.5	0.78	1.3	45.4	0.64
E	2.69	94.1	1.31	2.2	76.9	1.08
F	3.76	131.8	1.85	3.1	107.6	1.52

CTDI, CT dose index; DLP, dose length product; ED, effective dose.

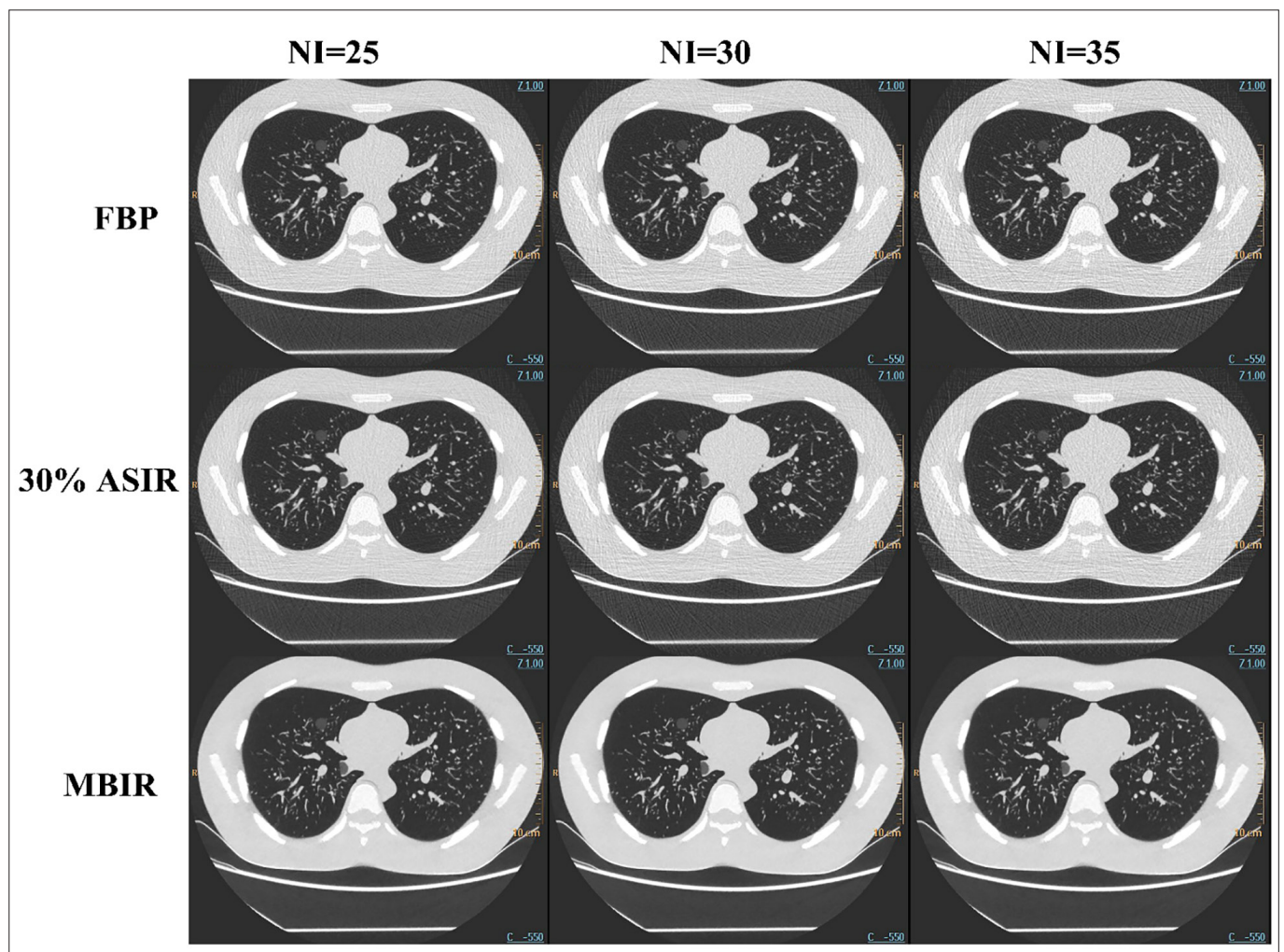


Figure 2. Comparison of image quality with reconstruction by the filtered back projection (FBP), 30% adaptive statistical iterative reconstruction (ASIR), and model-based iterative reconstruction (MBIR) algorithms with noise index (NI) values of 25, 30, and 35 at a tube voltage of 80 kV on the HDCT scanner.

Table 2. CT values of lung air and homogeneous thorax obtained with the HDCT and iCT scanners at 80 kV

Group	CT value of lung air					CT value of homogeneous thorax tissue				
	FBP (1)	30% ASIR	MBIR	F	P	FBP (1)	30% ASIR	MBIR	F	P
A (n=6)	-986.92±6.52	-985.78±6.41	-965.92±18.31	5.993	0.012*	-36.72±19.54	-37.68±16.44	-10.30± 5.90	6.327	0.010*
B (n=6)	-986.50±14.34	-991.75±8.59	-989.70±4.94	0.415	0.668	-23.92±4.65	-41.3±10.88	-28.80±6.68	7.837	0.005*
C (n=6)	-961.75±30.58	-934.95±16.19	-987.77±5.06	10.264	0.002*	-44.38±15.76	-32.67±15.66	-27.62± 9.68	2.266	0.138
F value	3.158	46.542	8.147			4.587	2.953	11.141		
P value	0.072	0.000*	0.004*			0.101	0.083	0.001*		
	FBP (2)	iDOSE ⁴ L3	iDOSE ⁴ L6			FBP (2)	iDOSE ⁴ L3	iDOSE ⁴ L6		
D (n=6)	-963.46±16.01	-969.83±24.88	-973.05±24.03	0.353	0.708	-138.96±27.27	-111.86±20.40	-116.97±4.79	3.154	0.072
E (n=6)	-969.40±33.12	-989.30±8.94	-991.42±8.59	2.123	0.154	-47.80±12.17	-60.68±7.00	-50.02±15.98	1.886	0.186
F (n=6)	-973.50±29.83	-990.55±13.81	-990.10±6.98	1.502	0.254	-18.11±7.57	-24.57±4.80	-25.19±5.05	2.611	0.106
F value	0.205	2.729	2.404			75.215	70.901	133.465		
P value	0.817	0.098	0.124			0.000*	0.000*	0.003*		

CNR, contrast-to-noise ratio; FBP(1), filtered back projection of HDCT; ASIR, adaptive statistical iterative reconstruction; MBIR, model-based iterative reconstruction algorithm. *P < 0.05.

Table 3. Average noise and CNR values in images reconstructed at 80/100 kV with the HDCT scanner

Group	Average noise					CNR				
	FBP (1)	30% ASIR	MBIR	F	P	FBP (1)	30% ASIR	MBIR	F	P
80 kV										
A	28.03±3.53	23.53±2.64	18.59±12.32	2.344	0.130	7.20±3.38	8.67±4.02	13.89±6.91	2.949	0.083
B	29.92±7.14	26.88±3.93	11.15±2.57	25.017	0.000*	6.84±3.45	7.70±3.69	18.93±5.70	14.117	0.000*
C	32.97±5.27	28.42±16.79	11.14±1.98	7.611	0.005*	6.47±3.66	8.69±5.51	18.81±6.21	9.459	0.002*
F value	1.223	0.369	2.048			0.066	0.094	1.256		
P value	0.322	0.698	0.163			0.937	0.911	0.313		
100 kV										
A	24.73±5.17	20.85± 6.64	10.47±2.60	12.605	0.001*	9.19±5.09	11.06±5.32	26.86±15.59	5.706	0.014*
B	31.09±7.48	21.43±7.40	11.37±1.95	15.293	0.000*	6.63±2.43	11.18±4.88	18.37±5.08	11.344	0.001*
C	40.38±4.49	30.06±20.17	10.55±1.56	9.620	0.002*	5.00±2.36	8.44±3.89	20.27±7.35	15454	0.000*
F value	10.854	0.946	0.341			2.150	0.642	1.107		
P value	0.001*	0.410	0.716			0.151	0.540	0.356		

CNR, contrast to noise ratio; FBP(1), filtered back projection of HDCT; ASIR, adaptive statistical iterative reconstruction; MBIR, model-based iterative reconstruction algorithm. *P < 0.05.

above-average or substantial image noise that may interfere with diagnostic decision-making in less than half of the lung parenchyma; and 5, above-average or substantial image noise that may interfere with diagnostic decision-making

in more than half of the parenchyma. Diagnostic acceptability of the GGNs was evaluated on a four-point scale: 1, a fully acceptable image on which GGNs could be easily detected in the whole lung; 2, a probably acceptable image on which

GGNs could be easily detected in at least one area of the lung; 3, an inferior image on which GGNs were difficult to detect in at least one area of the lung; 4, an unacceptable image on which GGNs were difficult to detect in the whole lung.

Table 4. Average noise and CNR of reconstructed images by different algorithms and NI at 80 or 100 kV with the iCT scanner

Groups	Average noise					CNR				
	FBP (2)	iDOSE ⁴ L3	iDOSE ⁴ L6	F	P	FBP (2)	iDOSE ⁴ L3	iDOSE ⁴ L6	F	P
80 kV										
D	104.08±21.03	80.58±20.92	60.38±12.47	8.319	0.004*	2.41±0.77	3.19±0.99	4.15±1.42	3.793	0.046*
E	89.93±49.45	58.77±16.78	49.24±14.7	2.626	0.105	3.25±1.42	4.74±1.68	5.70±2.55	2.425	0.122
F	62.80±28.04	47.71±19.09	34.03±10.21	2.972	0.082	4.35±1.14	5.86±1.33	6.76±3.86	1.479	0.259
F value	2.137	4.645	6.618			4.353	5.825	1.324		
P value	0.153	0.027*	0.009*			0.032	0.013*	0.296		
100 kV										
D	67.58±16.25*	48.81±7.25	42.92±13.30*	6.050	0.012*	3.61±1.09	5.27±1.83	6.44±2.99	2.712	0.099
E	55.38±17.82	45.00±18.61	36.46±13.91	1.884	0.186	4.83±0.90*	6.51±1.97	7.56±1.57*	4.752	0.025*
F	46.07±11.69*	40.66±9.30*	27.13±1.74*	7.572	0.005*	6.17±3.09	5.98±3.55	10.03±3.56	2.702	0.099
F value	2.917	0.617	3.034			2.584	0.349	2.524		
P value	0.085	0.553	0.078			0.110	0.711	0.114		

CNR, contrast to noise ratio; NI, noise index; FBP, filtered back projection.
**P* < 0.05.

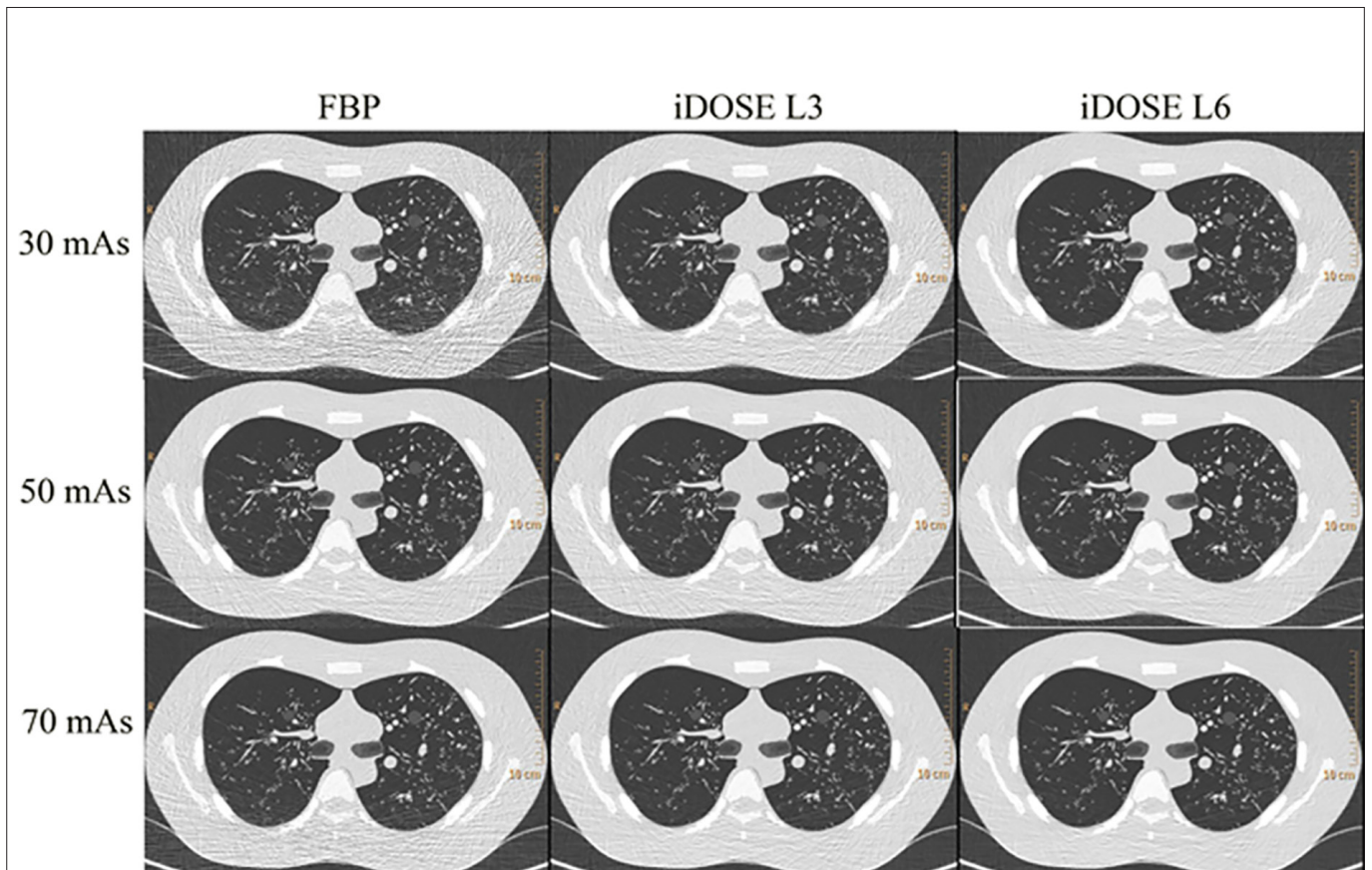


Figure 3. Comparison of the quality of images obtained using the FBP, iDOSE⁴ L3, or iDOSE⁴ L6 reconstruction algorithms with three tube currents at 80 kV with the iCT scanner.

Table 5. Kappa coefficient of subjective score of image quality evaluation in each Group from observers 1 and 2 on the HDCT and iCT scanners at 80 kV

Group	Subjective noise, k(c)						Diagnostic acceptability, k(c)					
	FBP(1)	P	30% ASIR	P	MBIR	P	FBP(1)	P	30% ASIR	P	MBIR	P
A (n=8)	0.867	≤0.001	0.840	≤0.001	0.826	≤0.001	0.889	≤0.001	0.692	≤0.001	0.826	≤0.001
B (n=8)	0.862	≤0.001	1.000	NA	0.826	≤0.001	0.886	≤0.001	1.000	NA	0.840	≤0.001
C (n=8)	1.000	NA	0.714	≤0.001	0.714	≤0.001	0.714	≤0.001	0.862	≤0.001	0.840	≤0.001
	FBP(2)		iDOSE ⁴ L3		iDOSE ⁴ L6		FBP(2)		iDOSE ⁴ L3		iDOSE ⁴ L6	
D (n=8)	0.750	≤0.001	0.867	≤0.001	0.886	≤0.001	0.840	≤0.001	0.857	≤0.001	0.886	≤0.001
E (n=8)	0.862	≤0.001	0.867	≤0.001	0.886	≤0.001	0.714	≤0.001	0.879	≤0.001	0.879	≤0.001
F (n=8)	0.867	≤0.001	0.886	≤0.001	0.879	≤0.001	0.867	≤0.001	0.846	≤0.001	0.840	≤0.001

FBP(1), filtered back projection of HDCT; FBP(2), filtered back projection of iCT; ASIR, adaptive statistical iterative reconstruction; MBIR, model-based iterative reconstruction algorithm.

Statistical analysis

Differences in average noise and CNR values between groups A through F and pairwise comparison between groups were determined by using multivariate analysis of variance by using Bonferroni *post hoc* analyses with SPSS 19.0 (SPSS Inc.). The agreement of subjective evaluation of image quality between two observers was assessed by using MedCalc version 15.6.1 (MedCalc Software). Kappa coefficients, $k(c)$, with different levels of subjective image quality evaluation were classified as follows: $0 < k(c) < 0.40$, poor; $0.40 \leq k(c) < 0.59$, fair; $0.60 \leq k(c) < 0.74$, good; $0.75 \leq k(c) < 1$, excellent (24). P value < 0.05 was considered statistically significant.

Results

Radiation doses of the HDCT and iCT scanners at tube voltages of 80 and 100 kV were shown in Table 1. As the NI increased, the tube current decreased, and the dose index, DLP, and ED gradually decreased.

When the images were obtained on the HDCT at 80 kV and reconstructed with FBP, the CT values of the lung air and the homogeneous thoracic tissue were not significantly different among groups A, B, and C, as shown in Table 2. When the 30% ASIR algorithm or MBIR was used, there were significant differences in the CT values of lung air and homogeneous thorax tissue between groups C and A and groups A and B, respectively. In group A, significant differences were obtained in CT values of the lung air and homogeneous thoracic tissue when comparing between images reconstructed with the MBIR and 30% ASIR algorithms.

For images obtained on the iCT scanner at 80 kV, there was significant difference in the CT value of homogeneous thorax tissue with various reconstruction algorithms. No difference was observed in the CT values of lung air with various tube currents and reconstruction algorithms (Table 2). There were significant differences in the CT value of homogeneous thorax tissue with 30 mAs between iDOSE⁴ L6 and FBP and between iDOSE⁴ L6 and iDOSE⁴ L3.

Table 3 reports the average noise and CNR values obtained using different reconstruction algorithms on the HDCT scanner with tube voltages of 80 and 100 kV. The average noise of images obtained at 80 kV with an NI of 35 and MBIR was reduced by 66.2% or 60.8% compared with images reconstructed by FBP or 30% ASIR, respectively. Images reconstructed by FBP or 30% ASIR had larger average noise values than images reconstructed by MBIR when larger NI values were used. At an NI of 35, the average noise with MBIR was 40.1% less than the noise at an NI of 25, but similar to the noise at an NI of 30 (Fig. 2).

Using the HDCT scanner at 100 kV, the average noise value increased (Table 3) and CNR decreased with increasing NI for the same reconstruction algorithm. At the same NI, the average noise of images reconstructed by MBIR was significantly less than the noise of images reconstructed by FBP or ASIR. The average noise at an NI of 35 with MBIR was reduced by 73.9% or 64.9% compared with the average noise with the FBP or ASIR algorithm, but was approximately equal to the average noise with MBIR and an NI of 25. Statistically significant differ-

ences were obtained for average noise values between FBP and MBIR in groups A, B, and C at 80 and 100 kV ($P < 0.05$), between FBP and 30% ASIR in all three groups at 80 kV ($P < 0.05$), and between 30% ASIR and MBIR in group B at 80 kV and in group A at 100 kV ($P < 0.017$). The differences in CNR between FBP and MBIR, 30% ASIR and MBIR in group B and group C at 80 kV and 100 kV were statistically significant, respectively, and between FBP and 30% ASIR in group A at 80 kV was statistically significant.

Table 4 reports the average noise and CNR values of images obtained using the iCT scanner with different reconstruction algorithms, tube currents, and voltages. Image noise decreased and CNR increased with increasing tube current. When the tube current was constant, CNR increased and noise decreased as the reconstruction algorithms progressed from FBP to iDOSE⁴ L3 to iDOSE⁴ L6. At 80 kV, the average noise with iDOSE⁴ L6 algorithm was 45.8% less than with FBP reconstruction in group F and 67.3% less than with FBP reconstruction in group D. The average noise value with the iDOSE⁴ L6 algorithm in group F was 43.6% less than the average noise in group D (Fig. 3). The difference in average noise value between FBP and iDOSE⁴ L6, iDOSE⁴ L6 and iDOSE⁴ L3 in group D was statistically significant, respectively. The difference between FBP and iDOSE⁴ L3 and FBP, iDOSE⁴ L6 in group F was statistically significant. The differences in CNR between FBP and iDOSE⁴ L6, iDOSE⁴ L3 and iDOSE⁴ L6 in group D and between FBP and iDOSE⁴ L3 in groups E and F were statistically significant.

Reconstruction with iDOSE⁴ L6 resulted in minimal noise and the maximal CNR with

a tube voltage of 100 kV and a tube current of group F. The average noise with the iDOSE⁴ L6 algorithm was less than the average noise obtained with FBP by 41% and that of iDOSE⁴ L3 by 33.3%. In group F with iDOSE⁴ L6, the average noise was 59.9% and the CNR was 177.8% of that in group D with FBP. Comparing groups D and F, the noise in group F was 31.9% less with FBP, 16.7% less with iDOSE⁴ L3, and 36.8% less with iDOSE⁴ L6. Compared with the CNR in group D, the CNR in group F increased by 70.9% with FBP, 23.5% with iDOSE⁴ L3, and 55.7% with iDOSE⁴ L6. At 80 kV, the radiation doses of group A and group D were the same. The average noise of group A with MBIR was 69.21% lower than that of group D with iDOSE⁴ L6, and the CNR was increased by 70.12%. The difference in average noise values between FBP and iDOSE⁴ L3 in group D and E was statistically significant, and between FBP and iDOSE⁴ L6 in group E and F was statistically significant. The difference in CNR between FBP and iDOSE⁴ L3 in group D and between FBP and iDOSE⁴ L6 was statistically significant.

The Kappa coefficient, $k(c)$, of the subjective score for image quality evaluation from observers 1 and 2 in each group on the HDCT and iCT scanners at 80 kV was shown in Table 5. Based on the subjective noise, the scores from observers 1 and 2 were higher in groups A and B with MBIR than those in groups with FBP and 30% ASIR. The score from observers 1 and 2 in group F with iDOSE⁴ L6 was 4 and 5, respectively. The score of diagnostic acceptability in groups A and B with MBIR was 5 and 4, respectively, which were higher compared with those in other groups.

Good interobserver consistency in the scoring results was obtained ($k(c) = 0.910$). Significant differences were found in image noise and diagnostic acceptability of GGNs. Also, significant differences were observed in image quality and diagnostic acceptability of the GGNs in the FBP, 30% ASIR, MBIR at same NI and in the FBP, iDOSE⁴ L3, and iDOSE⁴ L6 at same tube current.

Discussion

Obtaining high-quality images with the lowest radiation dose possible (as low as reasonably achievable, ALARA, principle) remains a challenge for clinicians. CTDIvol for a shift-variant scan protocol with the particular constraints of similar E, DLP, and L approximates the average dose over the

scan length (25), and DLP is a function of both the scan range and the CTDIvol, which may vary for different types of scanners and different vendors (26). ED is calculated from the DLP by using a specific correction factor for the scan region. In our study, we found that CTDI and DLP were different between groups A and D with 80 kV, but ED was the same. Thus, the calculation of ED was required for dose tracking, comparing dose values from different examinations and modalities, and for further protocol optimization. Compared with imaging at 100 kV, x-ray penetration at 80 kV is weaker and skin absorption is greater, such that the ED exceeds that at 100 kV. Using a chest model to explore the image quality of different low-dose CT reconstruction algorithms on two different commercial CT scanners, it was found that the ED of the HDCT scanner at 100 kV was only 0.49 or 0.36 mSv with an NI of 30 or 35, respectively. Consequently, this type of examination should be suitable for low-dose lung cancer screening purposes. Radiologists often judge the nature of lesions by their CT values. However, few studies have examined how changes in the NI and reconstruction algorithm affect CT values. When the HDCT scanner was used with NI values of 35 and 25, images reconstructed with the 30% ASIR and MBIR algorithms yielded significantly different CT values. Differences in the radiation dose when using the ASIR and MBIR algorithms may affect the accuracy of the CT value measurements on the HDCT scanner.

Due to the small sample size and the lack of comparison of the CT values with regular doses in this study, additional studies on the IR algorithms are required. Nevertheless, the range of CT values was only about 6%, which was small enough not to affect the qualitative aspects of the images.

IR techniques are different from FBP and can selectively remove image noise, thereby producing better-quality images at lower radiation doses (17, 27). IR algorithms can meet the needs of clinical diagnostic CT of the chest and abdomen at lower doses (16, 23, 28, 29). Many IR techniques are currently in use clinically. The ASIR is based on statistical principles for iterative data-space and image-space calculations. Other IR algorithms, including MBIR and iDOSE⁴, are based on iterative arithmetic models that have been used in many noise and anatomical models of spatial and image projections for multislice CT data. MBIR incorporates

the system statistics model, physics model, and the system optical model, which can further significantly reduce the image noise, improve the spatial resolution, and reduce image artifacts (30–32).

The most important factor affecting image quality, image noise, can be represented as the SD of the CT value of a homogeneous material. Miéville et al. (18) evaluated the image quality of chest and abdomen models using the SD of the CT value as a metric. In this study, the CT value and SD of six GGNs and the perinodular background were measured to evaluate the image noise quantitatively using various reconstruction algorithms for images obtained with the HDCT and iCT scanners.

On the iCT scanners, noise reduction compared with the FBP algorithm was greater with the iDOSE⁴ L6 than with the iDOSE⁴ L3 algorithm. Even with an ED of 1.85 mSv, the iDOSE⁴ L6 algorithm significantly reduced image noise compared with the FBP algorithm, showing that the iDOSE⁴ algorithms had similar noise reduction capabilities regardless of radiation dose. Thus, the iDOSE⁴ algorithms could reduce image noise and improve the CNR to maximize the diagnostic quality of images. These conclusions were consistent with those of previous reports (33–35). The image average noise of HDCT with MBIR is significantly lower than that of iCT with iDOSE⁴ L6 in the same radiation dose. Klink et al. (36) reported that iDOSE⁴ did not significantly affect low-contrast resolution at all levels in comparison to FBP when using the same tube voltage and current. Deák et al. (30) reported superior low-contrast resolution found at 1.0% and 0.5% low contrast by using ASIR and MBIR with a phantom. Furthermore, MBIR offers better objective and subjective analysis than ASIR in some studies (37–39).

Automatic tube current modulation (ATCM) systems are now used for the majority of CT scans. The principles of ATCM operation were different between GE and Philips scanners. GE scanners base the current modulation on a target noise setting, whereas Philips scanners use reference image and reference mAs concepts (40, 41). The GE scanner with ATCM systems maintained constant image, but tube currents are dependent on patient size and showed greater variations in CTDIvol. ATCM slightly affected image quality because of the constant cross-sectional area of the model applied in our study. Given that the model ap-

plied in this experiment showed a constant cross-sectional area, ATCM slightly affected the image quality in this experiment. Sook-peng et al. (42) reported that patient doses from Philips scanners slightly increased with patient size, but noise was greater than that from GE scanners.

There were several potential limitations in our study. First, the results obtained from a phantom study cannot be directly applied to patients. The use of a phantom did not allow us to evaluate the influence of a chest wall, breathing or motion artifacts on image quality. Second, simulated nodules used in the phantom study were completely spherical in shape with homogeneous radiodensity, and IR can reduce noise more prominently in homogeneous tissue than in inhomogeneous tissue (43). Third, the body mass index of patients has an effect on image quality at lower radiation doses, so the results of this study cannot be applicable to overweight people. Fourth, in our study, we only evaluated and compared the levels of IR recommended by the vendors, the whole range of iterative strengths for the different algorithms are not comparable, but this was not the scope of this study. Finally, the number of GGNs in our study was relatively small, and the effects of nodule size and density on detection were not studied. So further prospective studies with a larger number of pulmonary nodules with different size and density needs to be carried out.

This study used the MBIR prototype but did not assess the computing speed of this algorithm because the reconstruction speed affected clinical practicality. Analyzed radiation doses ranged from 0.36 to 1.85 mSv. Future studies should examine further reductions in radiation dose for clinical CT. The MBIR and iDOSE⁴ IR techniques significantly reduce image noise and generate better image quality in low-dose CT. IR algorithms will be better integrated in clinical practice as computer technology improves and IR algorithms become streamlined.

In conclusion, different NI, tube current, or IR would not affect the accuracy of CT value. Three IR algorithms were able to reduce the image noise, and improve the image quality in low-dose CT. In the same radiation dose, the low-dose CT image quality reconstructed with MBIR is better than that of other IR algorithms. When using HDCT scanner, 100 kV, NI=30 or 35 scanning protocol should be suitable for low-dose lung cancer screening purposes.

Acknowledgments

This study was supported by Beijing Natural Science Foundation, China [Grant No. 7182040].

Conflict of interest disclosure

The authors declared no conflicts of interest.

References

1. Kraft M, Ibrahim M, Spector M, Forghani R, Srinivasan A. Comparison of virtual monochromatic series, iodine overlay maps, and single energy CT equivalent images in head and neck cancer conspicuity. *Clin Imaging* 2018; 48:26–31. [CrossRef]
2. Nagai H, Kim YH. Cancer prevention from the perspective of global cancer burden patterns. *J Thorac Dis* 2017; 9:448–451. [CrossRef]
3. Wang L, Yu C, Liu Y, Wang J, Li C, Wang Q, et al. Lung cancer mortality trends in china from 1988 to 2013: new challenges and opportunities for the government. *Int J Environ Res Public Health* 2016; 13:E1052. [CrossRef]
4. Law M, Ma WK, Lau D, Chan E, Yip L, Lam W. Cumulative radiation exposure and associated cancer risk estimates for scoliosis patients: Impact of repetitive full spine radiography. *Eur J Radiol* 2016; 85:625–628. [CrossRef]
5. Farioli A, Ottone M, Morganti AG, et al. Radiation-induced mesothelioma among long-term solid cancer survivors: a longitudinal analysis of SEER database. *Cancer Med* 2016; 5:950–959. [CrossRef]
6. Kim H, Park CM, Chae HD, Lee SM, Goo JM. Impact of radiation dose and iterative reconstruction on pulmonary nodule measurements at chest CT: a phantom study. *Diagn Interv Radiol* 2015; 21:459–465. [CrossRef]
7. Siegel MJ, Ramirez-Giraldo JC, Hildebolt C, Bradley D, Schmidt B. Automated low-kilovoltage selection in pediatric computed tomography angiography: phantom study evaluating effects on radiation dose and image quality. *Invest Radiol* 2013; 48:584–589. [CrossRef]
8. Schindera ST, Winklehner A, Alkadhi H, et al. Effect of automatic tube voltage selection on image quality and radiation dose in abdominal CT angiography of various body sizes: a phantom study. *Clin Radiol* 2013; 68:e79–86. [CrossRef]
9. Christner JA, Zavaletta VA, Eusemann CD, Walz-Flannigan AI, McCollough CH. Dose reduction in helical CT: dynamically adjustable z-axis X-ray beam collimation. *AJR Am J Roentgenol* 2010; 194:W49–55. [CrossRef]
10. Kang EJ, Lee KN, Kim DW, et al. Triple rule-out acute chest pain evaluation using a 320-row-detector volume CT: a comparison of the wide-volume and helical modes. *Int J Cardiovasc Imaging* 2012; 28(Suppl 1):7–13. [CrossRef]
11. Prezzi D, Goh V, Virdi S, Mallett S, Grierson C, Breen DJ. Adaptive statistical iterative reconstruction improves image quality without affecting perfusion CT quantitation in primary colorectal cancer. *Eur J Radiol Open* 2017; 4:69–74. [CrossRef]
12. Sorantin E, Riccabona M, Stucklschweiger G, Guss H, Fötter R. Experience with volumetric (320 rows) pediatric CT. *Eur J Radiol* 2013; 82:1091–1097. [CrossRef]
13. Andersen HK, Volgyes D, Martinsen ACT. Image quality with iterative reconstruction techniques in CT of the lungs—A phantom study. *Eur J Radiol Open* 2018; 5:35–40. [CrossRef]
14. Goodenberger MH, Wagner-Bartak NA, Gupta S, et al. Computed tomography image quality evaluation of a new iterative reconstruction algorithm in the abdomen (adaptive statistical iterative reconstruction-v) a comparison with model-based iterative reconstruction, adaptive statistical iterative reconstruction, and filtered back projection reconstructions. *J Comput Assist Tomogr* 2018; 42:184–190. [CrossRef]
15. Matsutomo N, Nagaki A, Sasaki M. Validation of the CT iterative reconstruction technique for low-dose CT attenuation correction for improving the quality of PET images in an obesity-simulating body phantom and clinical study. *Nucl Med Comm* 2015; 36:839–847. [CrossRef]
16. Xu Y, He W, Chen H, Hu Z, Li J, Zhang T. Impact of the adaptive statistical iterative reconstruction technique on image quality in ultra-low-dose CT. *Clin Radiol* 2013; 68:902–908. [CrossRef]
17. Rampinelli C, Origgi D, Bellomi M. Low-dose CT: technique, reading methods and image interpretation. *Cancer Imaging* 2013; 12:548–556. [CrossRef]
18. Mieville FA, Gudinchet F, Brunelle F, Bochud FO, Verdun FR. Iterative reconstruction methods in two different MDCT scanners: physical metrics and 4-alternative forced-choice detectability experiments—a phantom approach. *Phys Med* 2013; 29:99–110. [CrossRef]
19. Kuo Y, Lin YY, Lee RC, Lin CJ, Chiou YY, Guo WY. Comparison of image quality from filtered back projection, statistical iterative reconstruction, and model-based iterative reconstruction algorithms in abdominal computed tomography. *Medicine (Baltimore)* 2016; 95:e4456. [CrossRef]
20. Jia Y, Ji X, He T, et al. Quantitative analysis of airway tree in low-dose chest CT with a new model-based iterative reconstruction algorithm: comparison to adaptive statistical iterative reconstruction in routine-dose CT. *Acad Radiol* 2018; 25:1526–1532. [CrossRef]
21. Schonfeld SJ, Lee C, Berrington de Gonzalez A. Medical exposure to radiation and thyroid cancer. *Clin Oncol* 2011; 23:244–250. [CrossRef]
22. EUR 16262. European guidelines on quality criteria for computed tomography. www.drds.dk/guidelines/ct/quality/. Accessed 10 February, 2012.
23. Katsura M, Matsuda I, Akahane M, et al. Model-based iterative reconstruction technique for ultralow-dose chest CT: comparison of pulmonary nodule detectability with the adaptive statistical iterative reconstruction technique. *Invest Radiol* 2013; 48:206–212. [CrossRef]
24. Cicchetti DV. The precision of reliability and validity estimates re-visited: distinguishing between clinical and statistical significance of sample size requirements. *J Clin Exp Neuropsychol* 2001; 23:695–700. [CrossRef]
25. Dixon RL, Boone JM, Kraft RA. Dose equations for shift-variant CT acquisition modes using variable pitch, tube current, and aperture, and the meaning of their associated CTDI(vol). *Med Phys* 2014; 41:111906. [CrossRef]
26. Saltybaeva N, Jafari ME, Hupfer M, Kalender WA. Estimates of effective dose for CT scans of the lower extremities. *Radiology* 2014; 273:153–159. [CrossRef]
27. Singh S, Kalra MK, Gilman MD, et al. Adaptive statistical iterative reconstruction technique for radiation dose reduction in chest CT: a pilot study. *Radiology* 2011; 259:565–573. [CrossRef]

28. Bodelle B, Bauer RW, Holthaus L, et al. Dose and image quality of high-pitch dual source computed tomography for the evaluation of cervical lymph node status - comparison to regular 128-slice single source computed tomography. *Eur J Radiol* 2013; 82:e281–285. [\[CrossRef\]](#)
29. Vardhanabhuti V, Loader R, Roobottom CA. Assessment of image quality on effects of varying tube voltage and automatic tube current modulation with hybrid and pure iterative reconstruction techniques in abdominal/pelvic CT: a phantom study. *Invest Radiol* 2013; 48:167–174. [\[CrossRef\]](#)
30. Deak Z, Grimm JM, Treitl M, et al. Filtered back projection, adaptive statistical iterative reconstruction, and a model-based iterative reconstruction in abdominal CT: an experimental clinical study. *Radiology* 2013; 266:197–206. [\[CrossRef\]](#)
31. Dodge CT, Tamm EP, Cody DD, et al. Performance evaluation of iterative reconstruction algorithms for achieving CT radiation dose reduction - a phantom study. *J Appl Clin Med Phys* 2016; 17:511–531. [\[CrossRef\]](#)
32. Moloney F, Twomey M, James K, Kavanagh RG, Fama D, O'Neill S, et al. A phantom study of the performance of model-based iterative reconstruction in low-dose chest and abdominal CT: When are benefits maximized? *Radiography* 2018; 24:345–351. [\[CrossRef\]](#)
33. Pontana F, Pagniez J, Flohr T, Faivre JB, Duhamel A, Remy J, et al. Chest computed tomography using iterative reconstruction vs filtered back projection (Part 1): Evaluation of image noise reduction in 32 patients. *Eur Radiol* 2011; 21:627–635. [\[CrossRef\]](#)
34. Bulla S, Blanke P, Hassepass F, Krauss T, Winterer JT, Breunig C, et al. Reducing the radiation dose for low-dose CT of the paranasal sinuses using iterative reconstruction: feasibility and image quality. *Eur J Radiol* 2012; 81:2246–2250. [\[CrossRef\]](#)
35. Millon D, Vlassenbroek A, Van Maanen AG, Cambier SE, Coche EE. Low contrast detectability and spatial resolution with model-based iterative reconstructions of MDCT images: a phantom and cadaveric study. *Eur Radiol* 2017; 27:927–937. [\[CrossRef\]](#)
36. Klink T, Obmann V, Heverhagen J, Stork A, Adam G, Begemann P. Reducing CT radiation dose with iterative reconstruction algorithms: the influence of scan and reconstruction parameters on image quality and CTDIvol. *Eur J Radiol* 2014; 83:1645–1654. [\[CrossRef\]](#)
37. Botsikas D, Stefanelli S, Boudabbous S, Toso S, Becker CD, Montet X. Model-based iterative reconstruction versus adaptive statistical iterative reconstruction in low-dose abdominal CT for urolithiasis. *AJR Am J Roentgenol* 2014; 203:336–340. [\[CrossRef\]](#)
38. Staniszewska M, Chrusciak D. Iterative Reconstruction as a method for optimisation of computed tomography procedures. *Pol J Radiol* 2017; 82:792–797. [\[CrossRef\]](#)
39. Park SB, Kim YS, Lee JB, Park HJ. Knowledge-based iterative model reconstruction (IMR) algorithm in ultralow-dose CT for evaluation of urolithiasis: evaluation of radiation dose reduction, image quality, and diagnostic performance. *Abdom Imaging* 2015; 40:3137–3146. [\[CrossRef\]](#)
40. Martin CJ, Sookpeng S. Setting up computed tomography automatic tube current modulation systems. *J Radiol Prot* 2016; 36:R74–R95. [\[CrossRef\]](#)
41. Sookpeng S, Martin CJ, Cheebsumon P, Pengpan T. Practical experiences in the transfer of clinical protocols between CT scanners with different ATCM systems. *J Radiol Prot* 2017; 37:84–96. [\[CrossRef\]](#)
42. Sookpeng S, Martin C, Gentle D, Lopez-Gonzalez M. Relationships between patient size, dose and image noise under automatic tube current modulation systems. *J Radiol Prot* 2013; 34:103. [\[CrossRef\]](#)
43. Willemink MJ, de Jong PA, Leiner T, et al. Iterative reconstruction techniques for computed tomography Part 1: technical principles. *Eur Radiol* 2013; 23:1623–1631. [\[CrossRef\]](#)